We are IntechOpen, the world's leading publisher of Open Access books Built by scientists, for scientists

4,800
Open access books available

122,000
International authors and editors

135M
Downloads

Our authors are among the

154
Countries delivered to

TOP 1%
most cited scientists

12.2%
Contributors from top 500 universities

CLARIVATE ANALYTICS BOOK CITATION INDEX INDEXED

WEB OF SCIENCE™

Selection of our books indexed in the Book Citation Index in Web of Science™ Core Collection (BKCI)

Interested in publishing with us?
Contact book.department@intechopen.com

Numbers displayed above are based on latest data collected.
For more information visit www.intechopen.com

17

Lossless Operation in InP Mach-Zehnder Modulator Monolithically Integrated with Semiconductor Optical Amplifier

Yasuo Shibata and Takako Yasui
NTT Photonics Laboratories
Nippon Telegraph and Telephone Corporation
Japan

1. Introduction

There are a number of requirements for optical modulators used in large capacity photonic networks. They must be small, consume little power, operate at high speed, and be robust as regards fiber dispersion for long-haul transmission. Conventionally, lithium-niobate (LN) based modulators have been used in transmission systems. An InP Mach-Zehnder modulator (MZM) is attractive because it has a smaller chip size and lower driving voltage than an LN modulator [Rolland et al. (1993); Yoshimoto et al. (1999)]. Moreover, it has the potential for monolithic integration with a laser diode [J. S. Barton et al. (2003)]. We have been developing InP based MZMs, and have reported a 40 Gbit/s [Tsuzuki et al. (2006)] module and an 80 Gbit/s DQPSK modulator [Kikuchi et al. (2007)]. The drawback of the InP MZM is that the spot size of the device is only one-tenth that of an optical fiber, and the coupling loss between them through lenses cannot be reduced below 1.5 dB. Therefore, the insertion loss becomes larger than that when using LN modulators. Therefore we must find a way to compensate for both the coupling loss and the modulator insertion loss.

To achieve this, we monolithically integrated a semiconductor optical amplifier (SOA) with an InP n-p-i-n structure MZM. In this article, we describe the design, fabrication technology, and device performance of our SOA-integrated MZM (SOA-MZM). Fiber-to-fiber lossless operation is demonstrated across the entire C-band region. We also discuss the transmission characteristics of a 10-Gbit/s NRZ signal over a 100-km SMF, and the 200-km transmission of 10 Gbit/s optical duobinary signals.

This paper is organized as follows. Section 2 describes the device structure and fabrication processes. Section 3 presents the static characteristics of the fabricated device. Section 4 reports both dynamic and transmission characteristics. Section 5 contains our concluding remarks.

2. Device structure

The structure of the fabricated SOA-MZM device is shown schematically in Fig. 1. An SOA with a ridge waveguide structure and an MZM region with a high-mesa structure are monolithically integrated using the ridge-high-mesa butt joint technique [Kikuchi et al. (2002)]. The SOA has 8 periods of InGaAsP strained multiple quantum wells (MQWs) as an active layer, which is sandwiched between InGaAsP separated confinement heterostructure (SCH) layers. The MZM core is composed of 20 periods of InGaAsP/InP MQWs. The bandgap wavelengths of the MQW layers are set at 1550 nm for the SOA and 1430 nm for the MZM. In outline, the fabrication process is as follows: First, an SOA active layer and SCH layers are grown on an n-InP substrate. Next, all the layers are etched off except for the SOA region to form an SOA island, and then the MZM core layer, undoped InP cladding layer, thin p-doped layer, and n-doped cladding layer are butt-jointed. Next, a p-doped SOA cladding layer is grown. The p-cladding layer is removed from the MZM region, and an n-cladding layer is selectively grown. All crystal growth is performed using metalorganic vapor phase epitaxy (MOVPE). Then, an SOA stripe is dry etched using CH_4 reactive ion etching to form a ridge waveguide structure, and high-mesa passive waveguides forming a Mach-Zehnder interferometer are fabricated by using Br_2-N_2 reactive beam etching. The ridge waveguide of the SOA is 2.0 μm wide and 600 μm long. The width and height of the mesa in the MZM region are 2.0 and 3.5 μm, respectively. The SOA region and MZM region are joined using the ridge-high-mesa coupling technique. Both sides of the facet are anti-reflection (AR) coated. The 1.5-mm long dual phase modulator arms are equipped with electrodes with a lumped structure, which are terminated with a 50-Ωresistance. The total device size is 3.9 x 0.5 mm.

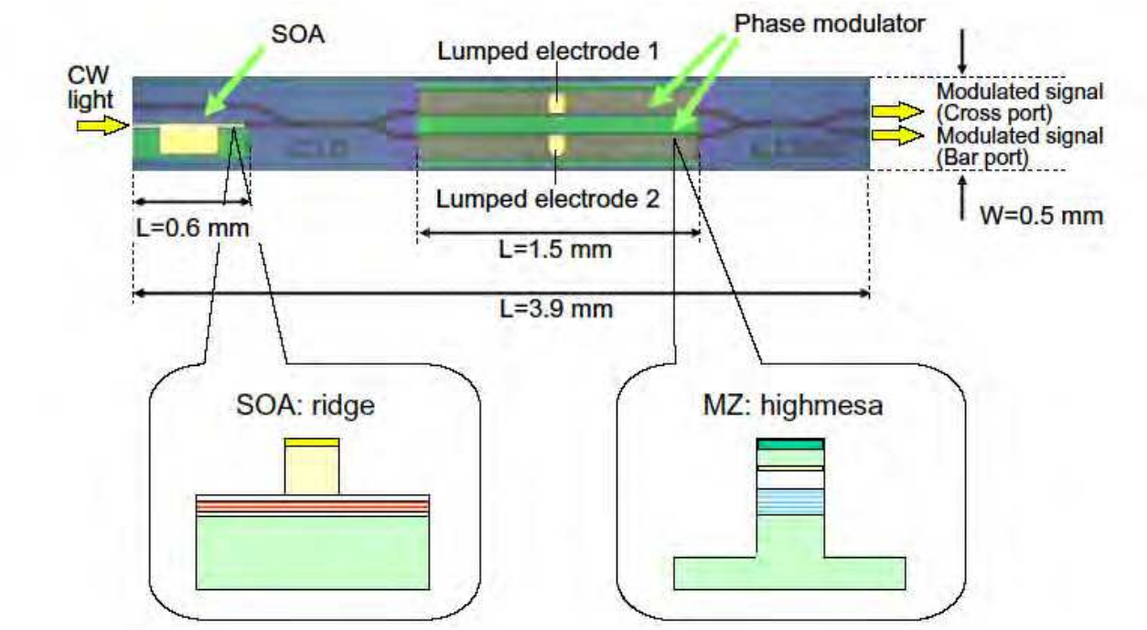

Fig. 1. Structure of the MZ-SOA

3. Static characteristics

The static optical characteristics of the monolithic device were investigated at 25 °C using TE polarized light focused with a lensed fiber on an AR-coated facet. The output light from the device was also collected by another lensed fiber. First, we examined the extinction characteristics under a single arm driving condition. Figure 2 shows the measured static extinction characteristics. Normalized optical transmissions from the MZM were plotted for input wavelengths of 1530, 1540, 1550 and 1560 nm as a function of the applied voltage (V_{b1}) to electrode 1 of phase modulator 1 in the upper arm while the bias voltage (V_{b2}) to electrode 2 of phase modulator 2 in the lower arm was held at 0 V. As shown in the figure, a half-wavelength voltage (V_π) of less than 2.5 V and a high extinction ratio (ER) of over 16 dB were obtained for the entire C-band region when the applied dc voltage was around 7 V. It is true that the extinction curves are asymmetric and the V_π value depends on both bias voltage and wavelength. This is because the refractive index change in a semiconductor material depends on the wavelength detuning between the bandgap wavelength and the input signal wavelength. It is also true that the detuning can be adjusted by adjusting the dc bias voltage, and therefore, the V_π value can be set at a constant value regardless of wavelength. Figure 3 shows an example of this condition. The normalized optical output of the SOA-MZM device for push-pull operation is shown in the figure. The horizontal axis indicates the difference between the applied voltage of the upper electrode and the bias voltage under a null condition in which the output optical power exhibits its minimum value. Under the null condition, the bias voltages applied to the upper and lower electrodes were 8.0 and 7.5 V, respectively, when the input wavelength was 1550 nm, and these values were adjusted according to the wavelength to keep the V_π value constant. From Fig. 3, V_π was 2.6 V and was constant for the entire C-band region.

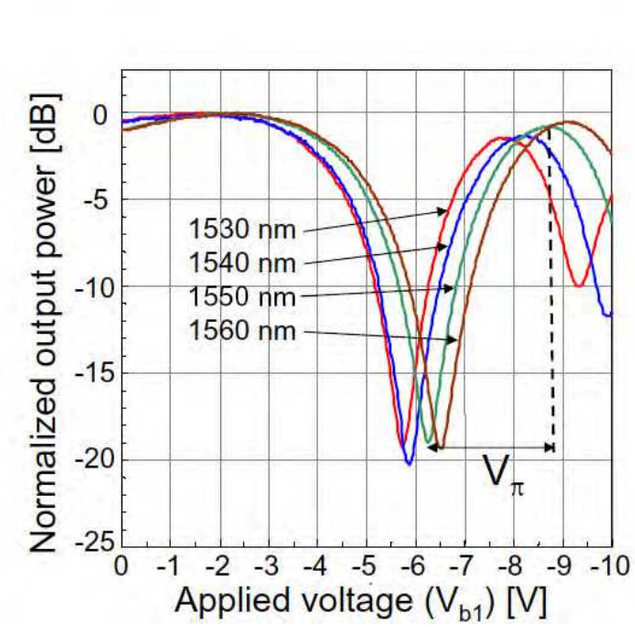

Fig. 2. Static extinction characteristics

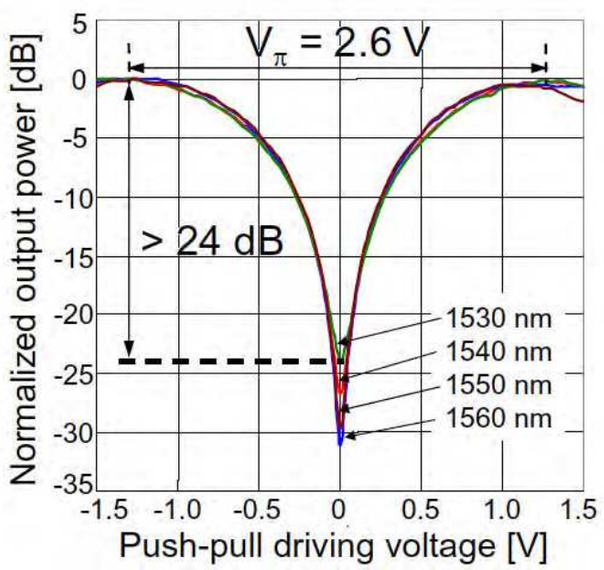

Fig. 3. Static extinction characteristics.

The extinction curves were completely symmetrical and identical, and the extinction ratio exceeded 24 dB for all wavelengths. These symmetrical characteristics indicate that the excess loss caused by the voltage-induced absorption (or electroabsorption) was negligible. These results reveal that this device has satisfactory characteristics for use in advanced modulation formats such as optical duobinary and differential phase shift keying signals.
We also investigated the gain characteristics of the integrated SOA. Figure 4(a) shows the fiber-to-fiber gain characteristics. The fiber output power was plotted against the fiber input power for a 1550-nm input signal while the upper and the lower arms of the MZM were held at 0 V. The coupling losses between the monolithic device and the lensed fiber were estimated to be 4 dB. The dashed line in the figure shows the fiber-to-fiber lossless condition, which means that the device gain exceeds 8 dB. The gain is sufficiently high to compensate for the 4 dB/facet fiber-coupling loss and the MZM insertion loss when the injection current exceeds 100 mA even when the input power is as high as -1.5 dBm. Furthermore, a large output power of over 6 dBm was obtained from the device with a 200 mA current injection when the input optical power into the device was -5.3 dBm. Figure 4(b) shows the device output power-SOA current characteristics for various input wavelengths across the C-band when the device input power was -8.6 dBm (the fiber input power was -4.6 dBm). We obtained both fiber-to-fiber lossless operation and operation with device gain for the entire C-band region at a current injection of 100 mA. And we obtained an output power of more than 4 dBm for all wavelengths with a 200 mA current injection.

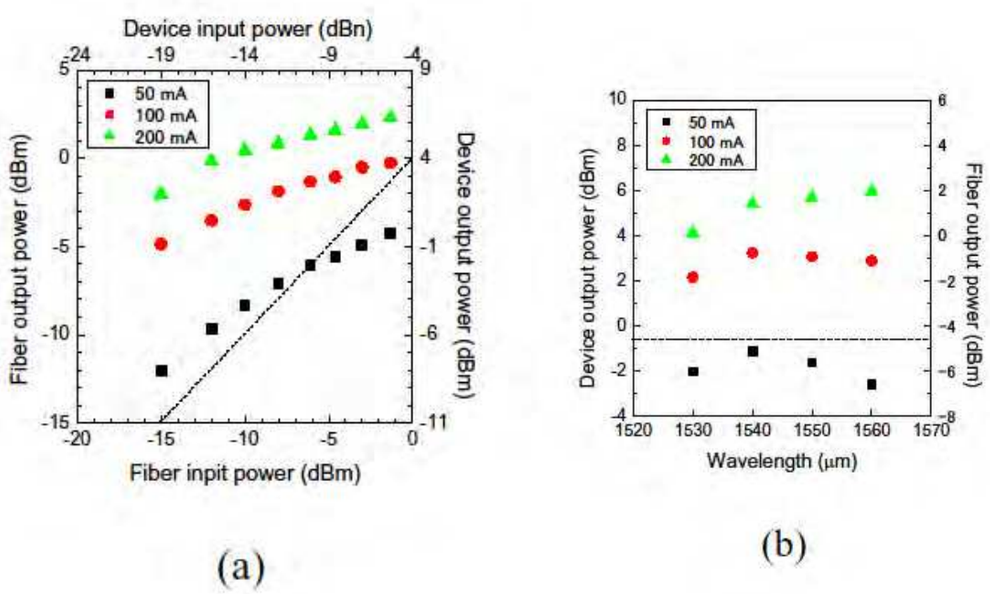

Fig. 4. Gain characteristics of the MZ-SOA. The input power dependence(a), and wavelength dependence(b).

4. Dynamic and transmission characteristics

The first topic in relation to the dynamic characteristics is the frequency response. Figure 5 shows the E/O response of the fabricated device. As seen in the figure, the 3-dB bandwidth was 7 GHz, which was large enough for 10-Gbit/s operation. Therefore, we then examined the transmission characteristics over an SMF at a bit rate of 10 Gbit/s.

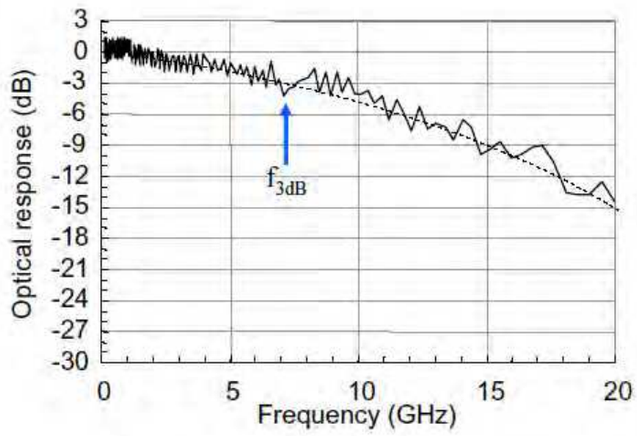

Fig. 5. Frequency response of the fabricated MZ-SOA.

The distance that optical signals can be transmitted through an SMF is limited by the group velocity (chromatic) dispersion of the SMF and the amount of spectral broadening (spectral width) of the optical signal. In principle, the optical spectrum is broadened when the optical intensity is coded by a high-speed digital signal. The spectrum experiences additional

broadening as a result of the instantaneous frequency change of the signal light, a phenomenon normally designated as 'chirp'. Therefore, frequency chirping is an important issue in any discussion of the dynamic modulation characteristics of a modulator. The amount of chirp is expressed by using a chirp parameter α_{cp}, and the parameter is defined by [Kawanishi et al. (2001)]

$$\alpha_{cp} = \Delta n / \Delta n' \tag{1}$$

where Δn and $\Delta n'$ are the relative changes in the real and imaginary parts of the complex refractive index, respectively.

It is well known that a negative chirp parameter of around -0.7 provides the best transmission distance results when using an NRZ intensity modulation format through an SMF fiber, while zero chirp is required for an advanced modulation format that utilizes phase information as well as intensity information such as the optical duobinary format. Therefore, we examined the dynamic modulation characteristics under two different driving conditions, namely a negative chirp condition and a zero chirp condition.

A. Negative chirp condition

We investigated the dynamic modulation characteristics when we applied a 2^{31}-1 pseudorandom binary sequence (PRBS) NRZ pattern at a bit rate of 9.953 Gbit/s to the MZM across the C-band. For the negative chirp driving condition, phase modulator 1 in the upper arm was dc biased and modulated with an NRZ signal of 3.0 V_{pp}, while phase modulator 2 in the lower arm was only dc biased to adjust the operation condition. The chirp parameter of the Mach-Zehnder modulator can be represented by

$$\alpha_{cp} = \frac{V_2 - V_1}{V_2 + V_1} \tag{2}$$

where V_1 and V_2 are the modulation (RF) voltages applied to electrode1 of phase modulator 1 in the upper arm and to electrode2 of phase modulator 2 in the lower arm, respectively. Under this driving condition, since phase modulator 2 in the lower arm was only dc biased, $V_2 = 0$. Therefore, according to equation (2), the calculated chirp parameter α_{cp} was -1. The fiber input optical power was -4.6 dBm, and the bias current to the SOA was 100 mA. Under this condition, the monolithic device had a signal gain of over 10 dB. Figure 6(a) shows electrically filtered back-to-back eye diagrams for the measured wavelength region of 1530 to 1560 nm. The waveforms were almost the same for the entire C-band region and the dynamic ER exceeded 9.6 dB for all wavelengths.

The bit error rate (BER) performance is shown in Fig. 7. Error free operation was confirmed for every wavelength. The wavelength dependence of the variation in received power sensitivity at a BER of 10^{-12} was less than 0.5 dB for the measured wavelength region. The transmission characteristics were then investigated using a 100-km long SMF. Electrically filtered eye diagrams after a 100-km transmission are shown in Fig. 6(b). Clear eye opening was obtained even after 100-km transmission. The BER characteristics of the transmitted signal are also shown in Fig. 7. As shown in the figure, no floor was observed in the BER

curve for any of the wavelengths, and error free operation after transmission was confirmed for every wavelength. The power penalty defined by the sensitivity degradation at a BER of 10^{-12} after a 100-km transmission was less than 1.5 dB across the C-band.

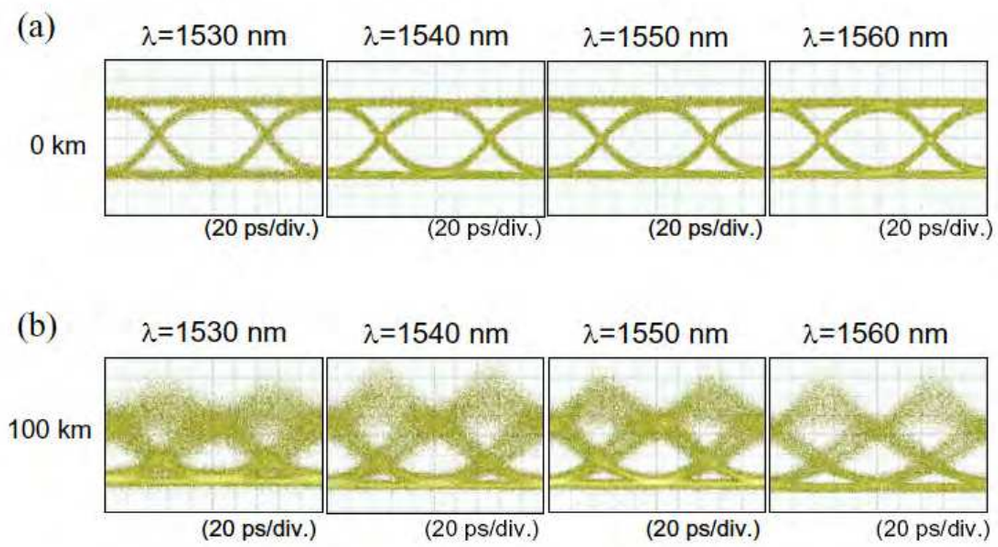

Fig. 6. Eye diagrams of back-to-back(a), and after 100-km transmission.

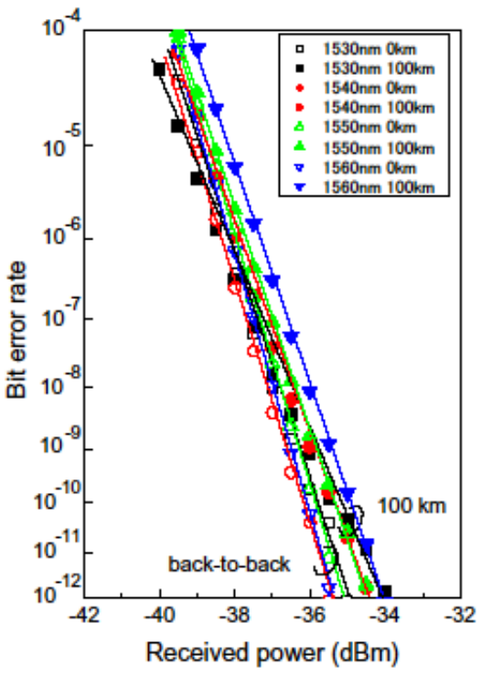

Fig. 7. Bit-error-rate characteristics for NRZ modulation.

B. Zero chirp condition

We examined the optical duobinary format for a zero-chirp driving condition [Yonenaga et al. (1997)]. The feature of an optical duobinary signal is its narrow spectral broadening compared with that of conventional non-return-to-zero (NRZ) modulation. An optical duobinary signal enables us to realize high-speed transmission with a large chromatic dispersion tolerance and a dense wavelength-division-multiplexing (DWDM) transmission with low adjacent channel crosstalk. Figure 8(a) is a diagram showing a method for generating an optical duobinary signal from a three-level electrical duobinary signal using an MZ modulator. A three-level electrical duobinary encoded signal ("-1", "0" and "1") is converted into a two-level optical duobinary signal ("1" and "0"), which is identical to the original binary signal inverted. The experimental setup is shown in Fig. 8(b). A TE polarized continuous-wave (CW) light is input into the dual-drive SOA-MZM using a lensed polarization maintaining fiber (PMF) with a coupling loss of 4 dB/facet. The optical duobinary signal is generated by differentially driving the MZM using three-level electrical signals with an amplitude of V_π while the MZM was dc biased at the null point where the optical output exhibits its minimum value without the RF modulation. As the modulation voltages were applied differentially, namely in a push-pull manner, $V_1 = V_2$, and therefore, according to equation (2), the calculated chirp parameter α_{cp} was 0. The three-level electrical signals were generated by low-pass filtering the 2^{31}-1 pseudorandom binary sequence (PRBS) NRZ signals at a bit rate of 9.953 Gbit/s with a cut-off frequency of 3 GHz. The output optical duobinary signals from the SOA-MZM were also coupled with the lensed SMF with a coupling loss of 4 dB. Following the 100-km SMF transmission, an erbium-doped fiber amplifier (EDFA) was employed to compensate for the fiber loss. The receiver consisted of an EDFA, an optical band-pass filter, a photodiode, and a clock and data recovery (CDR) circuit. The BER was measured using an error detector with the change of the input power into the receiver by a variable optical attenuator. The wavelengths of the CW light were 1550 nm. The temperature of the device was controlled at 25 ^{o}C. The transmission characteristics were investigated for SMF lengths of 0 (back-to-back), 60, 100, 160, and 200 km.

Figure 9(a) shows a back-to-back eye diagram of 10 Gbit/s optical duobinary signals using the SOA-MZM under the null condition shown in Fig. 3. Considering the electrical high-frequency loss at bias-T, and the connecting cables, the driving voltage was set at 2.8 peak-to-peak voltage (V_{pp}), which is slightly larger than the V_π value of 2.6 V shown in Fig. 3. The optical spectrum of the duobinary signal is shown in Fig. 9(b). We observed a narrow bandwidth with a 20-dB bandwidth of 13.6 GHz and no carrier frequency component, which is evidence that optical duobinary modulation was successfully realized with the fabricated MZ-SOA.

Figure 10(a) shows the measured eye diagrams for 10 Gbit/s optical duobinary signals after 60-, 100-, 160-, and 200-km SMF transmissions. Although chromatic dispersion degraded the eye opening as the transmission distance increased, clear eye opening was still obtained after a 200-km transmission. Figure 10(b) shows simulated results assuming a fiber dispersion of 16 ps/nm/km.

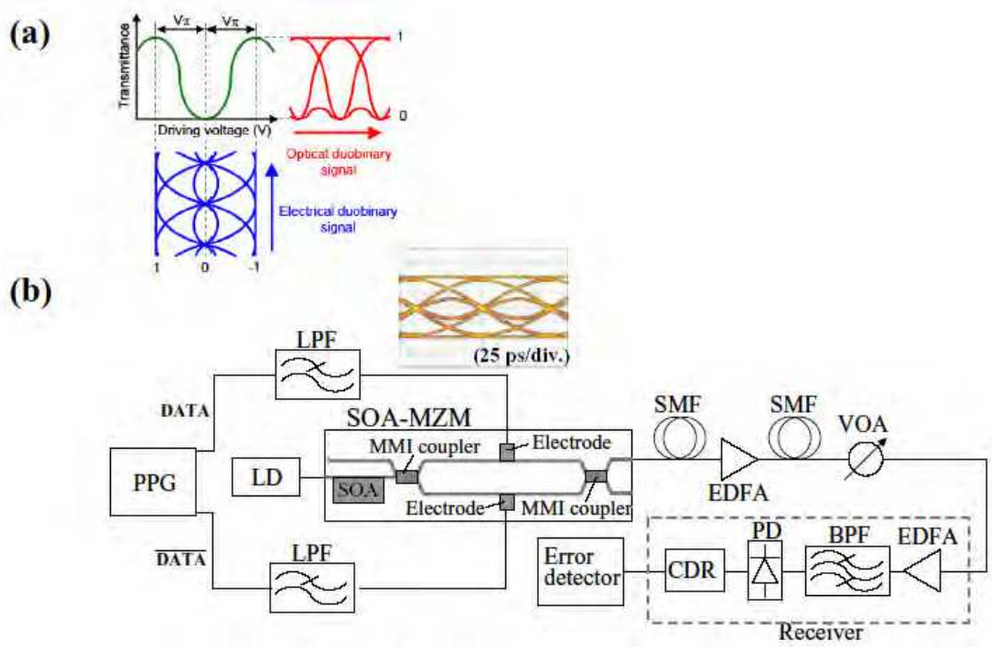

Fig. 8. Principle of generating optical duobinary signal (a), and experimental set-up (b).

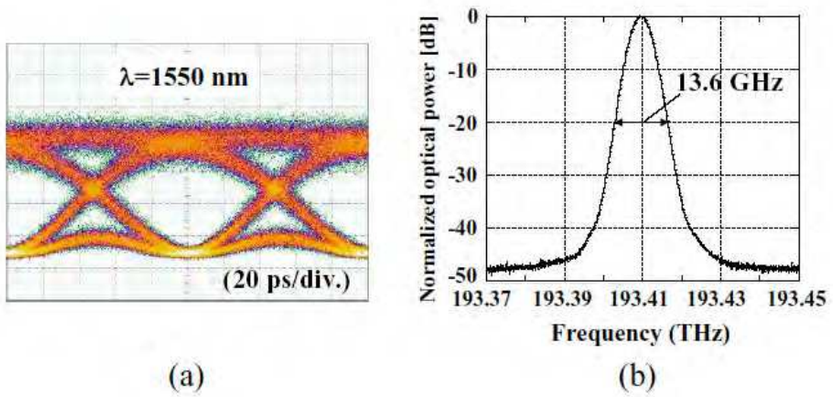

Fig. 9. Eye diagram (a) and optical spectrum (b) of the optical duobinary signal.

As can be seen, the experimental and simulation results are very similar for all distances, indicating the good quality of the modulator. Figure 11 shows the BER characteristics for all transmissions at a wavelength of 1550 nm. No floors were observed in the BER curves and error free operation was confirmed for all transmission distances. The power penalties defined by the sensitivity degradation at a BER of 10^{-12} were -0.7, -1.5, 0.4, 1.4 dB for 60-, 100-, 160-, and 200-km transmissions, respectively. These results are very similar to those obtained with a conventional (or non-integrated) MZ module [Kurosaki et al. (2007)], and therefore we can conclude that the monolithic integration process used in this work does not degrade the modulator quality. Figure 12 shows the wavelength dependence of the power penalty. The power penalty is less than -0.4, -1.4, 0.7, 2.3 dB for 60-, 100-, 160-, and 200-km transmissions, respectively, for the entire C-band region. These results prove that this

compact lossless MZM performs sufficiently well for application to optical duobinary transmission systems.

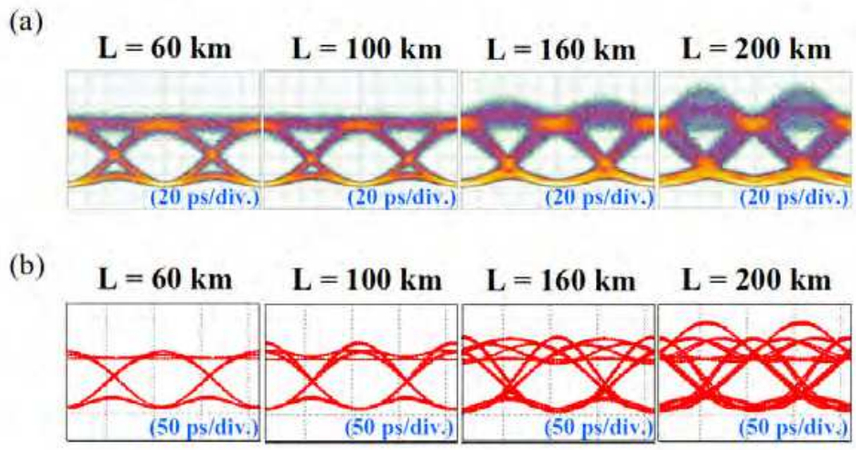

Fig. 10 Experimentally measured (a) and simulated (b) eye diagrams of optical duobinary signal after SMF transmission.

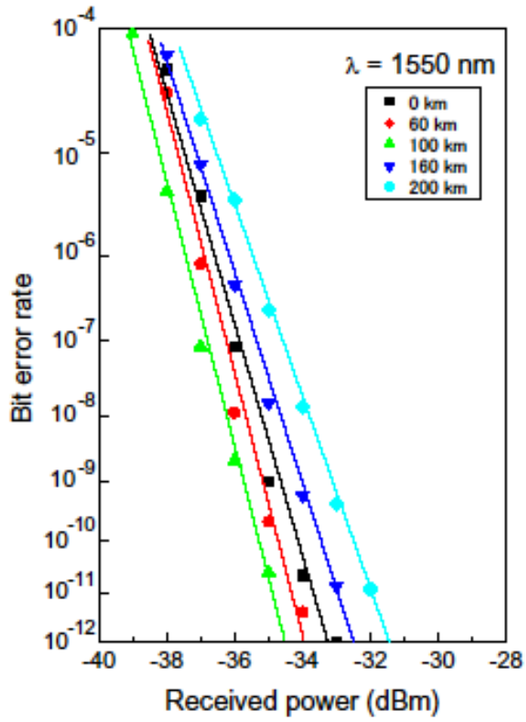

Fig. 11. Bit-error-rate characteristics for optical duobinary modulation.

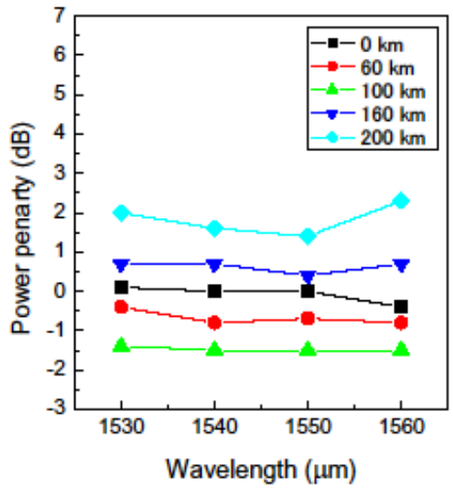

Fig. 12. Wavelength dependence of the power penalty.

5. Conclusion

An InP n-p-i-n MZM and an SOA were monolithically integrated to compensate for insertion loss. The device gain exceeded 10 dB, and fiber-to-fiber lossless operation was demonstrated for the entire C-band region. By using a lossless MZM, error free 100-km SMF transmissions were also demonstrated using an NRZ format at a bit rate of 10 Gbit/s for the entire C-band wavelength region. The measured power penalty after a 100-km transmission was only 1.5 dB.

10-Gbit/s optical duobinary transmissions were also demonstrated using the fabricated device. Lossless and error free operation was achieved with power penalties of less than -0.4, -1.4, 0.7, 2.3 dB for 0- (back-to-back), 60-, 100-, 160-, and 200-km SMF transmissions, respectively, at a low driving voltage of 2.8 V_{pp} for push-pull operation.

By comparing the experimental and simulation results, we confirmed that the modulation characteristics of this SOA-integrated lossless modulator are comparable to those of a discrete modulator. These results prove that this compact lossless MZM performs sufficiently well for application to optical duobinary transmission systems, and the integration process does not degrade modulator performance. These results constitute an important step towards achieving compact tunable light sources, realized by integrating a tunable laser and an MZM.

6. References

Barton, J. S.; Skogen, E. J.; Masanovic, M. L.; Denbaars, S. P. &Coldren, L. A. (2003). A widely tunable high-speed transmitter using an integrated SGDBR laser-semiconductor optical amplifier and Mach-Zehnder modulator. IEEE J. Sel. Topics Quantum Electron., 9, 1113-1117

Kawanishi, T.; Kogo, K.; Okikawa, S. &Izutsu, M. (2001). Direct measurement of chirp parameters of high-speed Mach-Zehnder-type optical modulators. Optics Communications, 195, 399-404

Kikuchi, N.; Shibata, Y.; Okamoto, H.; Kawaguchi, Y.; Oku, S.; Ishii, H.; Yoshikuni, Y. & Tohmori, Y. (2002). Error-free signal selection and high-speed channel switching by monolithically integrated 64-channel WDM channel selector. Electron. Lett., 38, 823-824

Kikuchi, N.; Sanjho, H.; Shibata, Y.; Tsuzuki, K.; Sato, T.; Yamada, E.; Ishibashi, T. & Yasaka, H. (2007). 80-Gbit/s InP DQPSK modulator with an n-p-i-n structure. 32nd European Conference on Optical Communication, Th10.3.1

Kurosaki, T.; Shibata, Y.; Kikuchi, N.; Tsuzuki, K.; Kobayashi, W.; Yasaka, H. & Kato, K. (2007). 200-km 10-Gbit/s optical duobinary transmission using an n-i-n InP Mach-Zehnder modulator. Proc. 19th IPRM, Matsue, Japan, May 14-18, WeB1-3

Rolland, C; Moore, R. S.; Shepherd, F. & Hillier, G. (1993). 10 Gbit/s, 1.56 μm multiquantum well InP/InGaAsP Mach-Zehnder optical modulator. Electronics Lett., 29, 471-472

Tsuzuki, K.; Kikuchi, N.; Sanjho, H.; Shibata, Y.; Kasaya, K.; Oohashi, H.; Ishii, H.; Kato, K.; Tohmori, Y. & Yasaka, H. (2006). Compact wavelength tunable laser module integrated with n-i-n structure Mach-Zehnder modulator. 31st European Conference on Optical Communication, Tu3.4.3

Yonenaga, K. & Kuwano, S. (1997). Dispersion-tolerant optical transmission system using duobinary transmitter and binary receiver. IEEE J. Lightwave Technol., 15, 1530-1537

Yoshimoto, N.; Shibata, Y.; Oku, S.; Kondo, S. & Noguchi, Y. (1999). Design and demonstration of polarization-insensitive Mach–Zehnder switch using a lattice-matched InGaAlAs/InAlAs MQW and deep-etched high-mesa waveguide structure. J.L.T, 17, 1662-1669

Semiconductor Technologies

Edited by Jan Grym

ISBN 978-953-307-080-3
Hard cover, 462 pages
Publisher InTech
Published online 01, April, 2010
Published in print edition April, 2010

Semiconductor technologies continue to evolve and amaze us. New materials, new structures, new manufacturing tools, and new advancements in modelling and simulation form a breeding ground for novel high performance electronic and photonic devices. This book covers all aspects of semiconductor technology concerning materials, technological processes, and devices, including their modelling, design, integration, and manufacturing.

How to reference

In order to correctly reference this scholarly work, feel free to copy and paste the following:

Yasuo Shibata and Takako Yasui (2010). Lossless Operation in InP Mach-Zehnder Modulator Monolithically Integrated with Semiconductor Optical Amplifier, Semiconductor Technologies, Jan Grym (Ed.), ISBN: 978-953-307-080-3, InTech, Available from: http://www.intechopen.com/books/semiconductor-technologies/lossless-operation-in-inp-mach-zehnder-modulator-monolithically-integrated-with-semiconductor-optica

INTECH
open science | open minds

InTech Europe
University Campus STeP Ri
Slavka Krautzeka 83/A
51000 Rijeka, Croatia
Phone: +385 (51) 770 447
Fax: +385 (51) 686 166
www.intechopen.com

InTech China
Unit 405, Office Block, Hotel Equatorial Shanghai
No.65, Yan An Road (West), Shanghai, 200040, China
中国上海市延安西路65号上海国际贵都大饭店办公楼405单元
Phone: +86-21-62489820
Fax: +86-21-62489821

IntechOpen